Mon. Not. R. Astron. Soc. **376,** L6–L10 (2007) doi:10.1111/j.1745-3933.2006.00274.x

# The carbon star IRC+10216: linking the complex inner region with its spherical large-scale structures

J.-L. Menut,[1⋆] E. Gendron,[2] M. Schartmann,[3] P. Tuthill,[4] B. Lopez,[1] W. C. Danchi,[5] S. Wolf,[3] A.-M. Lagrange,[6] S. Flament,[1] D. Rouan,[2] Y. Clénet[2] and N. Berruyer[1]

[1]*Gémini, Observatoire de la Côte d'Azur, 06304 Nice, France*
[2]*Laboratoire d'Etudes Spatiales et d'Instrumentation en Astrophysique (LESIA), Observatoire de Paris, 92195 Meudon, France*
[3]*Max-Planck-Institut für Astronomie, Königstuhl 17, 69117 Heidelberg, Germany*
[4]*School of Physics, University of Sydney, Sydney, NSW 2006, Australia*
[5]*NASA/Goddard Space Flight Center, Greenbelt, MD 20771, USA*
[6]*Laboratoire d'Astrophysique de l'Observatoire de Grenoble (LAOG), 38041 Grenoble, France*

Accepted 2006 November 29. Received 2006 November 8; in original form 2006 May 21

**ABSTRACT**

IRC+10216 is located at the tip of the asymptotic giant branch of the Hertzsprung–Russell diagram in a transition phase toward the post-asymptotic giant branch stage. Its study contributes to our knowledge of the late stage of stellar evolution of low- and intermediate-mass stars, when the circumstellar matter begins to adopt the asymmetric or bipolar forms commonly found in planetary nebulae. Using the NAOS–CONICA (NACO) adaptive optics system, we have mapped the circumstellar environment of IRC+1O216 at several wavelengths and three different epochs. The NACO study provides high-resolution and high-dynamic-range information on the different features displayed by the circumstellar envelope: clumpiness and a peanut- or bipolar-like shape at small scales. The link between the inner regions and the spherical-like shells observed at large scales is displayed in these high-dynamic-range data.

**Key words:** instrumentation: adaptive optics – stars: AGB and post-AGB – circumstellar matter – infrared: stars.

## 1 INTRODUCTION

The brief but spectacular final throes of the high-mass-loss process, in which the bulk of the stellar envelope is ejected, is a crucial step for stellar evolution and for the enrichment of the interstellar medium. For stars with initial mass between 1.4 and ∼8 $M_\odot$ on the main sequence, mass loss ensures that the stellar core never reaches the Chandrasekhar limit (1.4 $M_\odot$) and thus also has an impact on reducing the supernova rate.

The extreme carbon star IRC+10216 is a classical example of a red giant located at the tip of the asymptotic giant branch of the Hertzsprung–Russell diagram. It is evolving toward the post-asymptotic giant branch (post-AGB) stage. At 150 pc (Zuckerman, Dyck & Claussen 1986; Kastner 1992; Crosas & Menten 1997), this star is characterized by a high-mass-loss process, up to $10^{-5}\,M_\odot\,yr^{-1}$ (Mauron & Huggins 1999) and, therefore, is surrounded by an optically thick envelope. Actually, the star itself is so deeply embedded in its envelope that its precise location is subject to hypothesis (Men'shchikov, Hofmann & Weigelt 2002).

At large spatial scales, IRC+10216 displays a spherical wind and concentric dust shells (Mauron & Huggins 1999). These large-scale structures are observed as a result of the diffusion of the intergalactic stellar radiation field on to the dust shell, a phenomenon well reproduced through modelling (Mauron, de Laverny & Lopez 2003). However, this spherical symmetry seems to be broken when zooming in toward the core of the nebula (Weigelt et al. 1998, 2002; Tuthill et al. 2000; Tuthill, Monnier & Danchi 2005). These observations show that the core of the nebula is not far from a peanut- or a bipolar-like structure (Le Bertre, Magain & Remy 1989; Kastner & Weintraub 1994) in a clumpy environment.

The transition in the dust envelope between small-scale structures and large-scale ones is relevant for understanding the onset of asymmetry in the birth of post-AGB and planetary nebulae (bipolar winds, possible clumpiness in the envelopes). In particular, clumps are observed at a distance less than 0.2 arcsec from the centre of the nebula. At larger distances, according to the NAOS–CONICA (NACO) data that we present in this paper, the brightness profile in the image appears smoother.

Two hypotheses may actually explain this smoothness, despite the expectation that clumps are formed in the inner region and are transported by the stellar wind. These hypotheses are (i) the multiscattering of light in the dusty and clumpy medium, or (ii) the dilution of the clumps when moving away from the star.

After a presentation of the observations in Section 2, we discuss the relevance of these data in the remainder of this Letter. In order to

⋆E-mail: menut@obs-nice.fr

**Table 1.** Log of IRC+10216 NACO observations.

| Date | ESO filter | Remark | Seeing (arcsec) | Scale (arcsec pixel$^{-1}$) |
|---|---|---|---|---|
| 2002 Jan 27 | *Ks*, NB2.17 & IB2.27 | Br$\gamma$ line | ∼0.8 | 0.027 |
| 2002 Nov 22 | NB1.64 & *Ks* | – | ∼0.6 | 0.013 |
| 2003 Mar 15 | *J*, NB1.64 & *Ks* | [Fe II] line | ∼0.6 | 0.013 |

understand better the structural changes of the brightness map and the link between the rough small-scale and smooth large-scale structures, we compare these data with a preliminary radiative transfer model.

## 2 OBSERVATION AND DATA ANALYSIS

IRC+10216 was observed at three epochs: on 2002 January 27, on 2002 November 22 and on 2003 March 15. All observations were done at the Very Large Telescope (VLT), with the NACO system (Lenzen et al. 1998; Rousset et al. 2000) on the Nasmyth B focus of Unit Telescope 4. We used several filters as shown in the log of observations (Table 1).

We used a standard reduction procedure: first, cleaning the images by replacing bad pixels (by interpolation), subtracting the dark current and the sky flux, and correcting the pixel-to-pixel gain variations (division of the image by a normalized image of the flat-field). The second part of the processing is the shift-and-add procedure: the images are magnified by a factor of 4 and interpolated, then superimposed by researching the maximum of cross-correlation. In a last step, the images are resized to the original resolution. The result of the processing for all IRC+10216 images and for one point spread function (PSF) image is shown in Fig. 1.

## 3 RESULTS AND DISCUSSION

Two objectives were planned for this research programme: (1) understanding the small-scale structural changes of the inner envelope, and (2) understanding the link between small-scale and large-scale structures. We qualitatively discuss these points in the following subsections.

### 3.1 The small-scale structural changes of the inner envelope

Based on Keck aperture masking observations (*HKL* bands) and Special Astrophysical Observatory bispectrum speckle interferometry (*JHK* band), it was shown that the clumps of dust are moving as a result of the expanding wind of the star (Tuthill et al. 2000, 2005; Weigelt et al. 1998, 2002). All these observations cover periods between 1995 and 2002. The dust outflow speed is 17.5 km s$^{-1}$, and the clump velocity motions vary between 7.9 and 17.5 km s$^{-1}$ (Tuthill et al. 2000). In four months, some features in the envelope moved as much as 8.5 mas. In 2005, Keck aperture masking data (Tuthill et al., private communication) showed that the so-called North-East Arm elongated and strongly faded. The fading of the North-East Arm [especially the component B in the nomenclature of Haniff & Buscher (1998)] has already been reported by Weigelt et al. (2002). This phenomenon could be linked to the formation of new dust near the star, reducing the illumination of the North-East Arm. Compared with the reconstructed images by

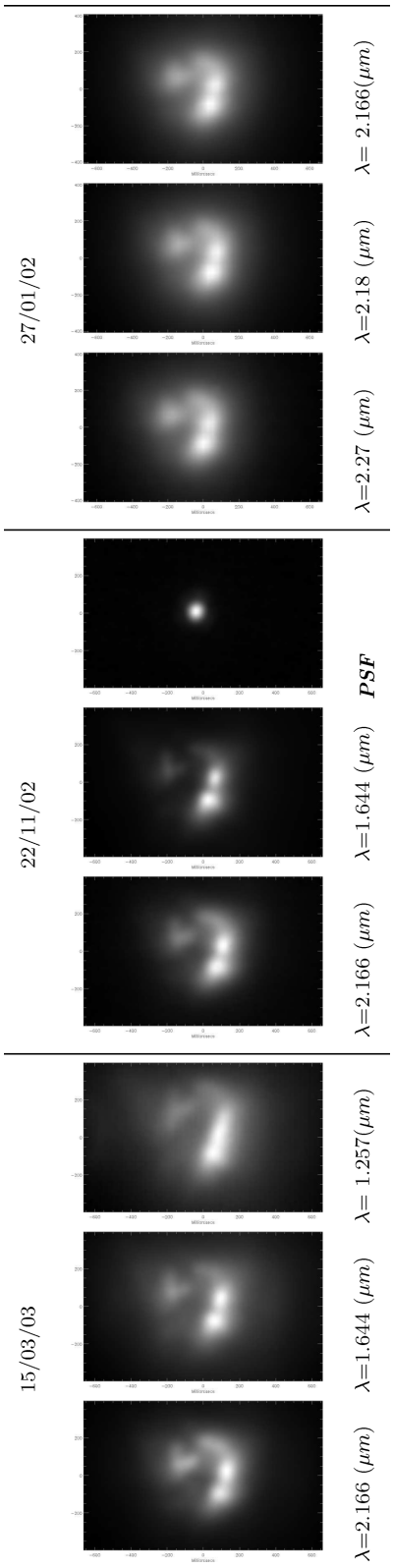


**Figure 1.** This figure shows the different IRC+10216 images, classified by date and wavelength of observation. The field of view is 600 mas (horizontally) by 400 mas (vertically). The first of the 2002 November 22 images displays the PSF.

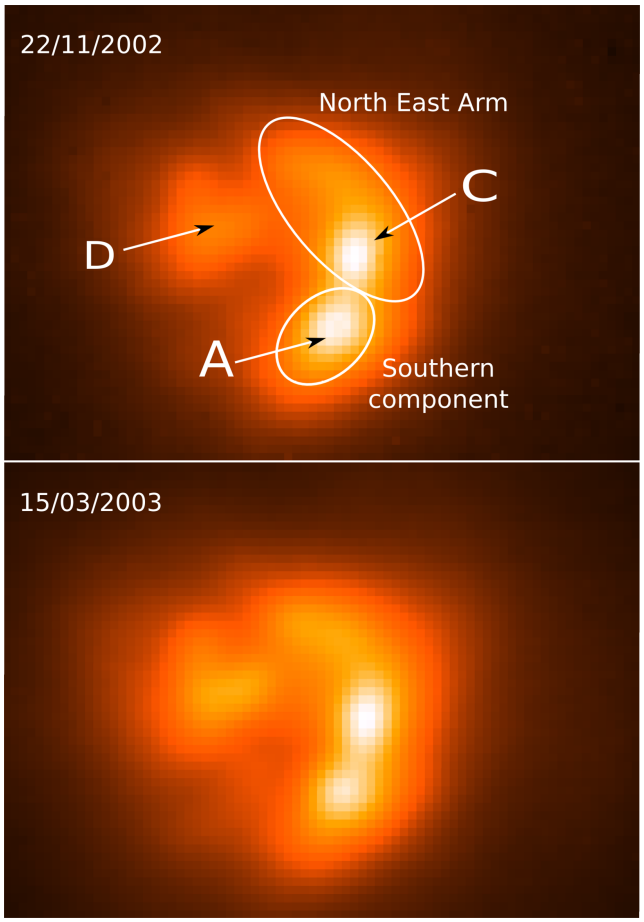


**Figure 2.** Zoom of IRC+10216 (top: image of 2002 November 22; bottom: image of 2003 March 15, both at 2.166 μm) showing its clumpy core, in particular the southern component and the North-East Arm (less bright). We used the notation from Haniff & Buscher (1998). The field of view is 0.7 × 1 arcsec$^2$. We notice that the core is surrounded by a smoother area and that the southern component became fainter in four months. The B clump seen by Tuthill et al. (2005) is not visible here.

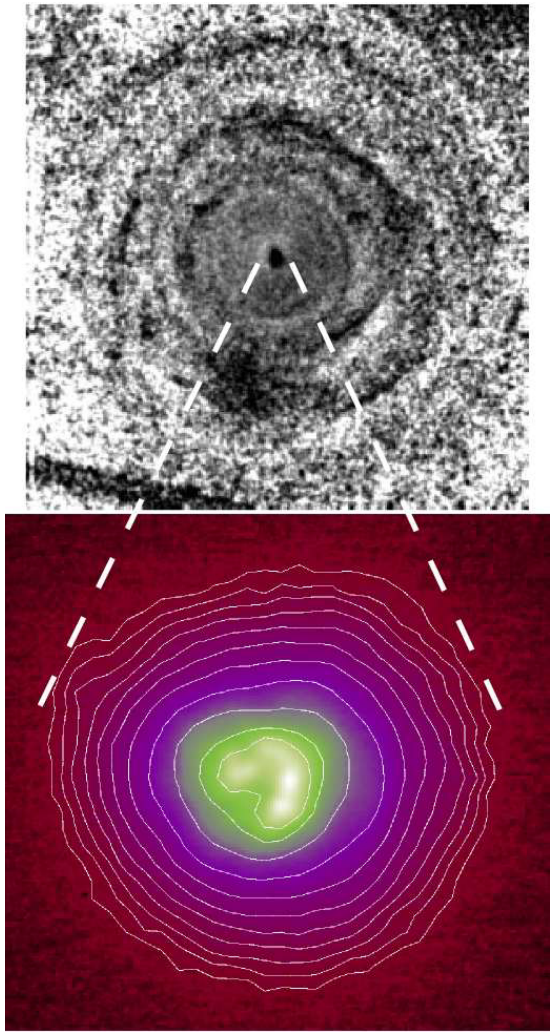

**Figure 3.** Top: composite $B + V$ image of IRC+10216 from Mauron & Huggins (1999). The field of view is about 130 arcsec. Bottom: 2.166-μm NACO image of IRC+10216. The total field of view is 2.3 × 2.7 arcsec$^2$ (∼ half of the central black area of the composite image). The lower level flux of IRC+10216 comes from a zone of ∼2 × 2 arcsec$^2$ (the last contour). The field of the clumpy and bright core is contained in a zone of 0.4 arcsec diameter (the first contour).

Tuthill et al. (2000) (in their fig. 1), our images show a faded and somewhat more curved North-East Arm (Figs 1 and 2) and a bright nodule has appeared at the beginning of this arm.

The NACO images in Figs 1 and 2 show the good agreement between high-resolution imaging with adaptive optics and other methods such as aperture masking. It is a confirmation that adaptive optics techniques are very suited to recovering complex structures at the full diffraction limit.

In Fig. 2, we notice the change in the brightness of the two bright nodules called A and C between 2002 November 22 and 2003 March 15: the relative brightness of C compared with A is 1.12 in 2002 and 1.44 in 2003. This change can be interpreted as being due to different mechanisms: (1) the illumination of the star changing in one direction; (2) some dust evaporation which happened between the star and clump A; and (3) additional nucleation and dust growth which occurred inside A.

### 3.2 The link between small-scale and large-scale structures

We want to understand the onset of the bipolar wind, supposed to occur during the transition between the AGB and post-AGB stages. The envelope of IRC+10216 appears spherical at large scales (see top panel of Fig. 3) while small-scale structures may trace the onset of a non-spherical (bipolar?) wind. The study of the connection between sphericity and core asymmetries can take advantage of the high dynamic range provided by adaptive optics. For instance, at 2.166 μm, a roughness is seen in the inner region (radius less than 0.3 arcsec) and a low-brightness envelope is in the background with an apparent extension of 2 arcsec, considering the signal-to-noise ratio of the image: the right-hand panel of Fig. 5 (later) shows the brightness profile of the inner region at a wavelength of 2.166 μm.

Two hypotheses may actually explain the change from roughness at small scales to smoothness at large scales in the envelope.

(i) A dynamical effect: dust clumps dilute while they move, transported by the wind.

(ii) A radiative transfer effect: the multiscattering of the stellar and dust-emitted photons. The clumps close to the star and near the hot inner dust region are easily seen; the others are in the shadow

of the first ones and multiscattering events tend smooth the contrast brightness.

Which hypothesis explains how the roughness observed at small scales changes into a smooth brightness distribution at larger scales? Are we observing a bipolar wind originating in the core? Or is it just an effect of non-isotropic dust formation?

In the latter case, the backwarming hypotheses may explain the sphericity at large scales: a dust clump is at one moment near the star; the backwarming process warms the region between the star and the clump, inhibiting new dust formation in this specific region, until the clump has moved away or faded enough. However, dust clump formation is still possible in any other direction where the amount of nearby clumps and backwarming is reduced. This process can repeat over a long period, thus creating a roughly spherical symmetric shell. When we look close to the star, we have access to the short-term evolution so that this process does not have time to take effect, and only the few inner clumps are visible.

### 3.3 Radiative transfer modelling

Some preliminary modelling has been done to give qualitative information about the previous hypotheses.

#### *3.3.1 Model parameters*

The density distribution of our models consists of two components. One component is a spherical envelope, from 15 au (the sublimation radius with a dust grain temperature of 1300 K) up to 300 au in radius (an arbitrary external limit in our models). Within the envelope, dust is continuously distributed with a radial dependence proportional to $r^{-2}$. Embedded in this medium, the second component is composed of 500 spherical clumps, with 10 to 100 times the local density and the same radius as the central star. They are placed at random positions uniformly distributed within the envelope volume. The enclosed dust mass is chosen such that the total optical depth at 11 μm reaches $\tau_{11\ \mu\mathrm{m}} = 1.3$ averaged over all lines of sight within the equatorial plane [optical depth compatible with spherical models of IRC+10216 by Danchi et al. (1994)]; some other models were also computed with 1/10 of the dust mass. For a summary of the main model parameters, see Table 2. The star is modelled as an extended (6 au in radius) primary energy source, which isotropically illuminates the dust shell with a 2000-K blackbody spectrum. A Lambertian emission by the stellar surface is assumed. For all simulated images and flux distributions, we assume a distance to the object of 150 pc (Zuckerman et al. 1986; Kastner 1992; Crosas & Menten 1997). The dust consists of the BE sample of amorphous carbon [optical data from Zubko et al. (1996)]. Effective characteristics of the dust grain are determined for a distribution of grain sizes between 0.2 and 1 μm with a number density distribution proportional to the power of −3.5.

**Table 2.** Parameters of the model.

| | | | |
|---|---|---|---|
| $R_{\mathrm{sub}}$ | 15 au | $R_{\mathrm{out}}$ | 300 au |
| $\rho_{\mathrm{cont}}$ | $\propto r^{-2}$ | $\langle\tau^{\mathrm{equ}}_{11\ \mu\mathrm{m}}\rangle_\phi$ | 1.3 |
| $N_{\mathrm{clump}}$ | 500 | $r_{\mathrm{clump}}$ | 6 au |
| $\rho_{\mathrm{clump}}/\rho_{\mathrm{cont}}$ | 100 | $d$ | 150 pc |
| Dust | amorphous carbon | $n(a)$ | $\propto a^{-3.5}$ |

For the simulations, we deploy MC3D (Wolf, Henning & Stecklum 1999), a three-dimensional continuum radiative transfer code based on the Monte Carlo approach. It is able to manage arbitrary three-dimensional dust and/or electron configurations and different primary sources of radiation. Working in the particle picture, the bolometric luminosity of the central source is divided into photon packages (weighted photons). They are fully characterized by their wavelength λ and their Stokes vector, describing the intensity and the polarization state of the photon (package). Photon packages are emitted according to a provided radiation characteristic (isotropic in the case of the present simulations) and spectral energy distribution of the source. Absorption, anisotropic (multiple) scattering and thermal dust re-emission are taken into account in the subsequent simulation of the radiative transfer in the surrounding envelope. In a last step, these packages are detected after leaving the model space. According to this procedure, temperature distributions as well as – in a second step – spectral energy distributions and surface brightness distributions are calculated.

Details on MC3D and the built-in features can be found in Wolf et al. (1999), Wolf & Henning (2000) and Wolf (2001, 2003). Pascucci et al. (2004) and Schartmann et al. (2005) tested MC3D for 2D structures against various other continuum radiative transfer codes, and found a good agreement.

#### *3.3.2 A qualitative model*

One of our simulated images is presented in Fig. 4. We selected this model among several, because the profile of the simulated image is comparable to the profile of the observations (see Fig. 5). As shown in the profile, the central roughness is due to the partial masking by clumps of the star and the bright inner edge of the envelope. The intensity profile then decreases smoothly away from the centre without showing roughness related to the distant clumps. This peculiar model is able to describe qualitatively the current observations, but other sets of parameters may also produce similar behaviour. Additional observational data from the MIDI interferometer are under analysis.

More detailed modelling is planned using a coherent approach based on combining NACO and MIDI data.

## 4 CONCLUSIONS OF THE FIRST ANALYSIS

The carbon star IRC+10216, mapped at 1.27, 2.17 and 2.27 μm in 2002 and 2003 with NACO, exhibits brightness contrast and

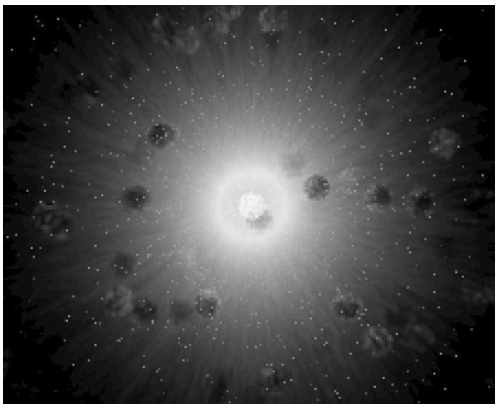

**Figure 4.** Simulated image at 2.2 μm. The field of view is about 19 × 16 stellar radii; the intensity scale is logarithmic.

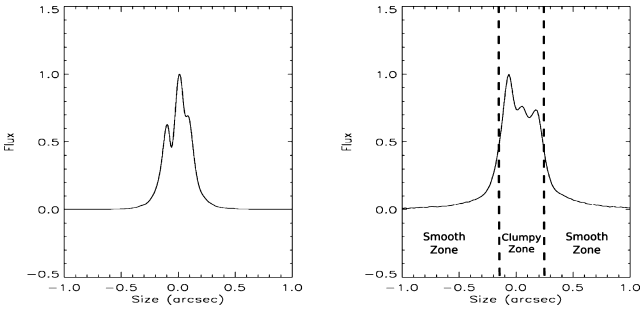


**Figure 5.** Left: intensity profile of a preliminary dust clump 3D radiative transfer modelling of IRC+10216. Right: section of the core of the image observed on 2003 March 15 at 2.166 μm. The total scale is 4 arcsec. The maximum flux value is normalized in order to be compared; the model profile is convolved with a PSF profile.

morphological changes (in the clumps and on the North-East Arm). Thanks to their high dynamic range, NACO images allow us to study the link between the clumpy and asymmetrical core and the smooth and spherical environment. A radiative transfer model with 500 clumps displays a similar behaviour.

## REFERENCES

Crosas M., Menten K. M., 1997, ApJ, 483, 913
Danchi W. C., Bester M., Greenhill L. J., Degiacomi C. G., Townes C. H., 1994, Proc. SPIE, 2200, 286
Haniff C. A., Buscher D. F., 1998, A&A, 334, L5
Kastner J. H., 1992, ApJ, 401, 337
Kastner J. H., Weintraub D. A., 1994, ApJ, 434, 719
Le Bertre T., Magain P., Remy M., 1989, The Messenger, 55, 25
Lenzen R., Hofmann R., Bizenberger P., Tusche A., 1998, Proc. SPIE, 3354, 606
Mauron N., Huggins P. J., 1999, A&A, 349, 203
Mauron N., de Laverny P., Lopez B., 2003, A&A, 401, 985
Men'shchikov A. B., Hofmann K.-H., Weigelt G., 2002, A&A, 392, 921
Pascucci I., Wolf S., Steinacker J., Dullemond C. P., Henning Th., Niccolini G., Woitke P., Lopez B., 2004, A&A, 417, 793
Rousset G. et al., 2000, Proc. SPIE, 4007, 72
Schartmann M., Meisenheimer K., Camenzind M., Wolf S., Henning Th., 2005, A&A, 437, 861
Tuthill P. G., Monnier J. D., Danchi W. C., Lopez B., 2000, ApJ, 543, 284
Tuthill P. G., Monnier J. D., Danchi W. C., 2005, ApJ, 624, 352
Weigelt G., Balega Y., Bloecker T., Fleischer A. J., Osterbart R., Winters J. M., 1988, A&A, 333, L51
Weigelt G., Bloecker T., Hofmann K.-H., Men'shchikov A., Winters J. M., 2002, A&A, 392, 131
Wolf S., 2001, PhD thesis, University of Jena
Wolf S., 2003, Comput. Phys. Commun., 150, 99
Wolf S., Henning Th., 2000, Comput. Phys. Commun., 132, 166
Wolf S., Henning Th., Stecklum B., 1999, A&A, 349, 839
Zubko V. G., Mennella V., Colangeli L., Bussoletti E., 1996, MNRAS, 282, 1321
Zuckerman B., Dyck H. M., Claussen M. J., 1986, ApJ, 304, 401

This paper has been typeset from a TEX/LATEX file prepared by the author.